THE JOURNAL OF PHYSICAL CHEMISTRY C

Article

pubs.acs.org/JPCC

Reaction Mechanism of Nerve-Agent Hydrolysis with the $Cs_8Nb_6O_{19}$ Lindqvist Hexaniobate Catalyst

Robert C. Chapleski, Jr.,[†] Djamaladdin G. Musaev,[‡] Craig L. Hill,[§] and Diego Troya*[,†]

[†]Department of Chemistry, Virginia Tech, Blacksburg, Virginia 24061, United States

[‡]Cherry L. Emerson Center for Scientific Computation, Emory University, Atlanta, Georgia 30322, United States

[§]Department of Chemistry, Emory University, Atlanta, Georgia 30322, United States

Supporting Information

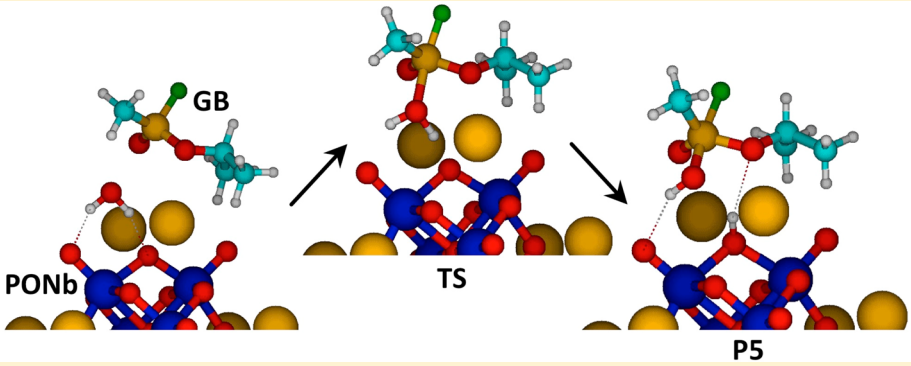

ABSTRACT: We present a detailed mechanism for the hydrolysis of Sarin catalyzed by $Cs_8Nb_6O_{19}$ obtained using electronic structure calculations. The initial steps of the reaction involve the adsorption of water and Sarin on the hexaniobate catalyst via nonbonding interactions. Dissociation of the coordinated water molecule generates a hydroxide ion that adds nucleophilically to the coadsorbed Sarin molecule in a concerted manner, following a general base catalysis mechanism. The addition of OH^- to the nerve agent generates a trigonal bipyramidal pentacoordinated phosphorus intermediate that subsequently undergoes facile dissociation forming either HF or isopropanol and a corresponding phosphonic acid. The rate-determining step of the overall reaction is found to be the dissociation of water on the catalyst in concert with the nucleophilic addition of the nascent OH^- to the nerve agent. The calculated barrier for this step is considerably smaller than that measured for bulk base hydrolysis. This work represents a blueprint for future studies aimed to optimize catalysts for base hydrolysis of nerve agents at the gas−surface interface.

INTRODUCTION

Interest in developing efficient catalytic decontamination strategies for chemical warfare agents remains unabated.[1,2] Early decontamination procedures employed a variety of general-purpose techniques ranging from bleaching to enzymatic biodegradation,[3] but many of these approaches required highly corrosive solution-phase treatments. More recently, the quest for improved decontamination processes has examined a number of solid-phase catalysts including zirconium hydroxide,[4] zeolites,[5] organic polymers,[6] polyoxometalates (POM),[7,8] metal−organic frameworks (MOF),[9−13] and MOF/POM architectures.[14,15]

Among the various classes of chemical warfare agents, nerve agents (e.g., Sarin, Soman, VX, Tabun) have arguably received the most attention in decontamination studies. These nerve agents consist of organophosphorus (OP) compounds with a central tetrahedral phosphorus atom. In vivo, these species inhibit acetylcholinesterase (a serine protease) following nucleophilic addition of the −OH group of a serine residue in the active site of the enzyme to the nerve agent.[16] The susceptibility of OP compounds toward nucleophilic addition has been exploited in the development of many of the catalysts mentioned above, which generally aim to decompose the OP species via base hydrolysis.[3]

Even though the experimental efforts to develop synthetic nerve-agent decontamination catalysts have been rather vigorous recently, there remains a lack of fundamental understanding of the fine details of their reaction mechanisms. Indeed, while the basic decontamination catalysts appear to involve general base hydrolysis,[7,11,12] the atomistic details of the formation of hydroxide on the catalyst, the addition of OH^- to the nerve agents, and the subsequent dissociation of the agents have not conclusively been revealed. This is in sharp contrast to the mechanism for nerve agents reacting with OH^- in bulk solution, which has received significant computational scrutiny.[17−19]

Received: June 1, 2016
Revised: July 8, 2016
Published: July 8, 2016

Downloaded via JOHNS HOPKINS UNIV on March 20, 2026 at 13:38:28 (UTC).
See https://pubs.acs.org/sharingguidelines for options on how to legitimately share published articles.

© 2016 American Chemical Society

DOI: 10.1021/acs.jpcc.6b05528
J. Phys. Chem. C 2016, 120, 16822−16830

There are two main mechanisms for catalytic base hydrolysis of a substrate in solution. In *specific* base catalysis, water is deprotonated to fully form a hydroxide ion in a first step, followed by nucleophilic attack of hydroxide on the substrate in a second step. In *general* base catalysis, the water deprotonation and nucleophilic addition to the substrate take place simultaneously. Recent work with Lindqvist hexaniobate alkali salts ($X_8Nb_6O_{19}$, X = Li, K, Cs) measured fast hydrolysis of Sarin both in aqueous solution and at the gas−surface interface.[7] Small-angle X-ray scattering (SAXS) measurements showed the aggregation of the OP compounds under study to the polyoxoniobate (PONb), which led to the suggestion that the reaction follows a general base catalysis mechanism. Finally, a study just published on the basic hydrolysis of nerve agents and their analogues, by polymeric polyniobates, $K_{12}Ti_2O_2XNb_{12}O_{40}$, X = Ge^{IV} or Si^{IV}, includes three lines of evidence that these PONbs, which share many molecular attributes in common with $Nb_6O_{19}^{8-}$, clearly hydrolyze these OP compounds by a general base catalyzed mechanism.[8]

In this article, we probe the general base catalysis reaction mechanism for the degradation of nerve agents on $Cs_8Nb_6O_{19}$ (CsPONb), using density functional theory (DFT) calculations. Computational work on the structure and reactivity of polyoxometalate catalysts has a rich history[20−26] and has been essential, in combination with synthetic and characterization approaches, to develop a profound understanding of the properties of these catalysts and to accelerate their discovery. Remarkably, most of the theoretical studies on POM reactivity have focused on acid, oxidation, and redox catalysis,[24] but there is a paucity of investigations of reactions in which the POMs act as base hydrolysis catalysts.

Of the wealth of POM catalysts that have been synthesized over decades,[27−36] Group-V POMs with Lindqvist ion structure, particularly $Nb_6O_{19}^{8-}$, are ideal candidates to act as base hydrolysis catalysts due to the high charge density of the exposed oxygen atoms.[37] It is therefore not surprising that alkali salts of the $Nb_6O_{19}^{8-}$ ion have recently been reported to hydrolyze nerve agents.[7,8] Computational work on $Nb_6O_{19}^{8-}$ has included structural studies using DFT methods,[38] the proposal (also with DFT methods) of an open-cage intermediate that leads to oxygen exchange with solvent measured with NMR,[39] and a recent molecular dynamics study of the protonation of $Nb_6O_{19}^{8-}$ in aqueous media.[40] However, no mechanistic studies of the base hydrolysis reactions with $Nb_6O_{19}^{8-}$ have been reported yet.

In this work, we aim to provide the groundwork for a full understanding of the decomposition of nerve agents over PONb and other catalysts by focusing on the reaction of Sarin with the alkali salt of the Lindqvist PONb, $Cs_8Nb_6O_{19}$, at the gas−surface interface. Experimental evidence for this heterogeneous reaction with well-characterized solid salts[41,42] of $Cs_8Nb_6O_{19}$ has been recently provided, as have related OP hydrolysis processes catalyzed by polymeric PONb.[8] While we are primarily interested in characterization of the reaction at the gas−surface interface, this work might also be applicable to the solution phase, as SAXS measurements indicate that in concentrated solutions of CsOH the Cs ions are in direct contact with the Lindqvist ion, without intervening solvent molecules (inner-sphere ion pairs).[43,44] This is in contrast to the K salts, where solvent-separated ion pairs are present. The aggregation of Cs ions to the niobates has also been reported in aqueous solution.[7] The presence of a contact ion pair between Cs and the PONb not mediated by solvent water molecules therefore might make the calculations herein more applicable to the solution-phase process with $Cs_8Nb_6O_{19}$ than with any other alkali PONb salt, even if the role of solvent in the homogeneous process is still unknown.

METHODS

All presented calculations have been carried out with the M06L density functional, as implemented in the Gaussian09 code.[45] Our choice of this functional is motivated by its ability to treat transition elements and noncovalent interactions accurately.[46] Geometry optimizations and harmonic normal mode calculations have used the 6-31G(d,p) basis set for the main-group elements and Lanl2dz basis set with associated effective core potentials for Nb and Cs atoms. Using these geometries, we have carried out single-point energy calculations with the [6-31++G(d,p) + Lanl2dz] basis set to further refine the energy. All reported energies in this article correspond to M06L/[6-31++G(d,p) + Lanl2dz] electronic energies corrected by the zero point. The stationary points were located using standard procedures and corroborated by harmonic frequency and intrinsic reaction coordinate analysis. We used an ultrafine integration grid to accelerate convergence of both wave function and geometry.

Most of our calculations consider dry hexaniobates in which only the water molecule that participates in the hydrolysis is present. A subset of the calculations incorporates explicitly 14 additional water molecules to make contact with experiment, which shows the presence of crystallizing water molecules.

RESULTS

Reagents. The reagents of the title reaction are the $Cs_8Nb_6O_{19}$ catalyst, H_2O, and Sarin (GB, propan-2-yl methylphosphonofluoridate). As seen in Figure 1, $Cs_8Nb_6O_{19}$ has octahedral point-group symmetry, and it possesses only five symmetry-inequivalent atoms: the central oxygen atom ($O_{central}$), six terminal O atoms ($O_{terminal}$), six Nb atoms, 12 bridging oxygen atoms ($O_{bridging}$), and eight Cs counterions. The distances between Nb and the $O_{central}$, $O_{terminal}$, and $O_{bridging}$ atoms are 2.407, 1.808, and 2.037 Å, respectively, in good agreement with values obtained from X-ray diffraction[41] of the $Cs_8Nb_6O_{19}$ tetradecahydrate salt (2.360, 1.804, and 1.987 Å, respectively). The radius of gyration of the salt calculated in this work as the root-mean-square displacement of all atoms from $O_{central}$ (3.62 Å) is also in good agreement with the experimental value of 3.6 Å.[43] The Cs counterions are interacting with the faces of the hexaniobate superoctahedron, and the distance between the Cs atom and the nearest $O_{bridging}$ atoms in the PONb is 2.948 Å.

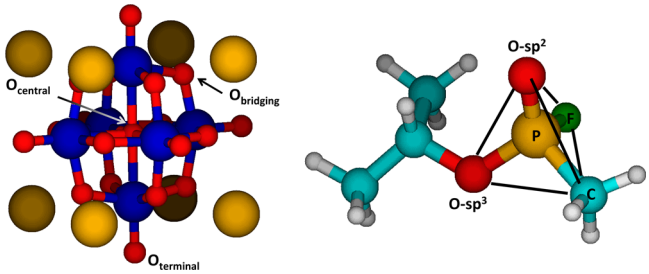

Figure 1. Optimum geometries of $Cs_8Nb_6O_{19}$ (left) and (*S*)-Sarin (GB, right). Color code: Nb, blue; O, red; Cs, gold; P, gold; C, cyan; F, green; H, white.

DOI: 10.1021/acs.jpcc.6b05528
J. Phys. Chem. C 2016, 120, 16822−16830

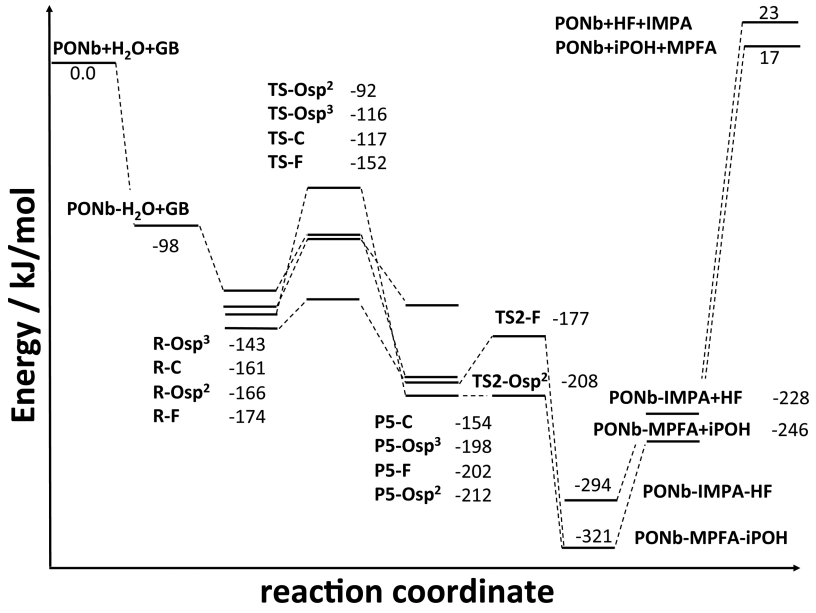

Figure 2. Potential energy profile for the hydrolysis of Sarin by $Cs_8Nb_6O_{19}$. See the text for the nomenclature used to label the various stationary points. Gibbs energies are available in Table S1.

Analysis of the standard Mulliken charges reveals the known trend in basicity of the various oxygen sites in the PONb: the calculated atomic charges are −0.943e, −0.994e, and −1.137e for the terminal, central, and bridging oxygen atoms, respectively. As shown in earlier experiments[47] and calculations,[40] the bridging oxygen is the most basic of the exposed atoms of the PONb.

Also depicted in Figure 1 is the optimum structure of (*S*)-Sarin, the enantiomer of higher toxicity[48] used in all calculations of this work. Highlighted in the figure is the tetrahedral shape around the central phosphorus atom, which undergoes nucleophilic addition of a hydroxide ion during the hydrolysis process. Because this atom is the stereogenic center of the molecule, there are, in principle, four symmetry-inequivalent approaches of hydroxide to the phosphorus atom. Nucleophilic addition to the tetrahedral OP compound generates a trigonal bipyramidal pentacoordinated species, and early work determined that the approach of lowest barrier is related to the apicophilicity of the substituent that is in an axial position in the forming trigonal bipyramid at the transition state.[49] The tendency of a group to occupy an axial position seems to have various contributions, including electronegativity, but also steric and inductive effects, and this makes it challenging to estimate a priori which one of the approaches might be the one of lowest energy. Below, we present reaction pathways and transition states for all four approaches.

Potential Energy Surface, Structure, and Energetics of the Calculated Intermediates, Transition States, and Products. The calculated potential-energy profile of the catalytic hydrolysis of Sarin by $Cs_8Nb_6O_{19}$ is shown in Figure 2. The elementary steps of this catalytic process are (i) binding of water to the CsPONb, (ii) binding of GB to the hydrated CsPONb, (iii) GB hydrolysis via formation of a pentacoordinated phosphorus intermediate, (iv) dissociation of the pentacoordinated intermediate into products bound to the CsPONb, and (v) desorption of products. In the following, we analyze each of these steps in turn.

Binding of Water to the CsPONb. The first step in the mechanism involves the binding of a water molecule to the catalyst to generate a CsPONb−H_2O complex. Of the two isomers located in this work (Figure S1), the most stable complex corresponds to a structure where H_2O binds in a bidentate manner to the CsPONb via two hydrogen bonds, one with a terminal O atom and the other with a neighboring bridging O atom. The calculated binding energy of this CsPONb complex is 98.3 kJ/mol (see Figure 2). Aside from the hydrogen bonds, we note that the oxygen atom of the water molecule is close to two Cs ions of the salt (O_{water}−Cs distances: 3.33 Å), which affords additional stabilization of the complex via electrostatic interactions.

CsPONb−H_2O−GB Complex. Once the CsPONb−H_2O complex is formed, the addition of the nerve agent leads to formation of CsPONb−H_2O−GB complexes (Figure 3). The four isomers of these complexes shown in the figure differ in the orientation of GB with respect to the CsPONb. We use the

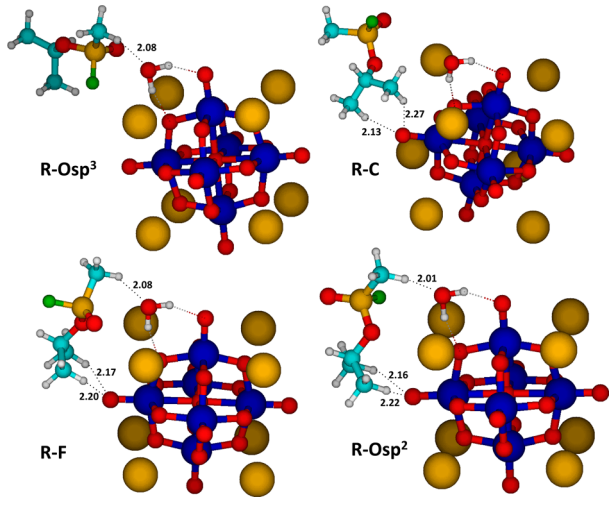

Figure 3. CsPONb−H_2O−GB complexes in which each of the faces of the central organophosphorus tetrahedron is interacting with CsPONb−H_2O. Numbers correspond to representative hydrogen-bond distances in Angstroms. Same color code as in Figure 1.

DOI: 10.1021/acs.jpcc.6b05528
J. Phys. Chem. C 2016, 120, 16822−16830

identity of the atom X whose P−X bond is collinear with the forming P−OH bond at the transition state to differentiate these isomers.

The formation of the CsPONb−H_2O−GB complexes is driven by dipole−dipole, dispersion, hydrogen-bonding, and electrostatic interactions between the Cs counterions and electron-rich atoms of the nerve agent. Key hydrogen-bond distances for these complexes are highlighted in Figure 3, and interactions between GB atoms and Cs counterions are shown in Figure S2. The binding energies of GB to the CsPONb−H_2O complex are 76.0, 67.7, 63.0, and 45.0 kJ/mol for isomers R−F, R−Osp^2, R−C, and R−Osp^3, respectively, and this ranking is related to the number of stabilizing interactions between GB and the hydrated CsPONb. For the most stable complex (R−F), we note the presence of two hydrogen bonds between GB and an $O_{terminal}$ atom of CsPONb, a hydrogen bond between GB and the adsorbed water molecule, and an electrostatic interaction between the O-sp^2 atom of GB and a Cs counterion (Figure S2).

Transition State for Water Deprotonation and OH Nucleophilic Addition to the Substrate. Following the potential energy profile of Figure 2, the next step of the general base catalysis is the concerted water deprotonation and OH nucleophilic addition to the nerve agent. This is the overall rate-determining step for GB hydrolysis by the CsPONb catalyst. Transition states for the four approaches examined in this work are exhibited in Figure 4, and movies of the atomic motions along the minimum energy reaction path for each pathway are available in the Supporting Information.

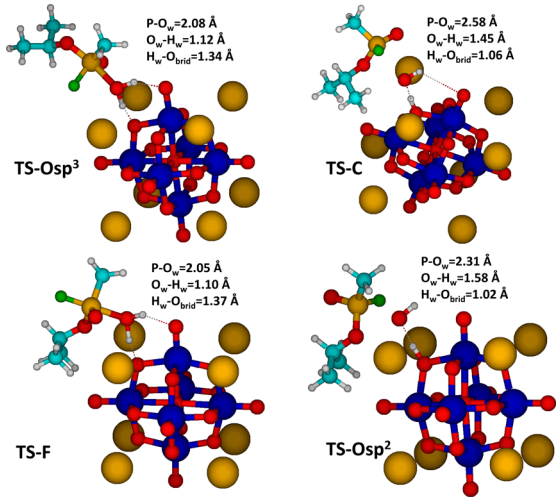

Figure 4. Transition state structures for the rate-determining step of the hydrolysis reaction of GB with CsPONb. Same color code as in Figure 1. Additional distances shown in Figure S3.

Figure 4 reveals that in all transition states, a nascent OH from the protonation of an $O_{bridging}$ atom in the CsPONb elicits nucleophilic addition to the nerve agent in a concerted manner. Interestingly, there are significant differences in the synchronicity of the protonation and addition motions. For instance, in TS-Osp^3 and TS-F, the OH addition is taking place while water is still not quite fully dissociated. However, in TS-C and TS-Osp^2, it seems that the OH group has been fully formed at the transition state, as the $O_{bridging}$ atom of the catalyst is protonated.

To better characterize these trends, we show in Figure 5 the evolution of the three key interatomic distances (the forming

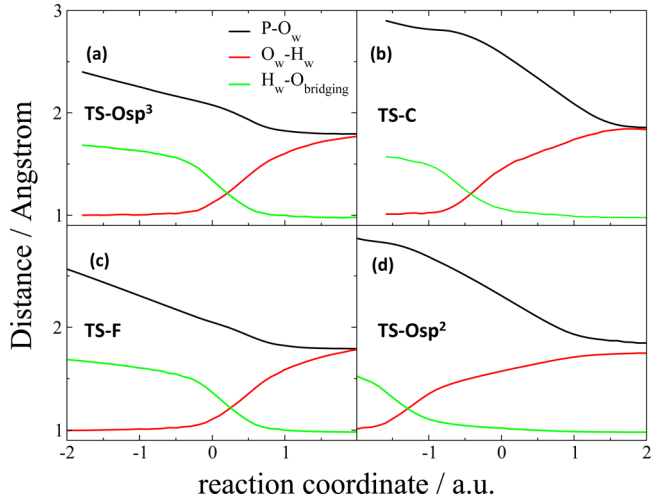

Figure 5. Evolution of the three key P−O_{water}, O_{water}−H_{water}, and $O_{bridging}$−H_{water} distances along the minimum energy reaction path for the rate-determining step in the four reaction paths of Sarin hydrolysis at an $O_{bridging}$ site examined in this work.

P−O_{water} and breaking O_{water}−H_{water} bonds, together with the $O_{bridging}$−H_{water} distance) along the minimum-energy reaction path for the four approaches considered in this work. The figure indicates that in the TS-Osp^3 and TS-F reaction paths, the water dissociation and CsPONb protonation are taking place at the same time that the P−O bond is forming, and at the transition state, all three bonds are in the process of either forming or breaking. However, for TS-C and TS-Osp^2, the protonation of the bridging oxygen seems to occur well before the transition state. This is particularly true for the TS-Osp^2 pathway, where the $O_{bridging}$−H_{water} bond is nearly fully formed by the time that the transition state is reached. Interestingly, the separation between the phosphorus atom and the nascent OH is also longer at the transition state for the reaction pathways of the transition states TS-C and TS-Osp^2.

The subtle differences in the atomic motions along the four minimum-energy reaction paths examined in this work appear to be correlated with the transition state energies calculated from the R complexes in Figure 3. Thus, while the energies for the TS-Osp^3 and TS-F transition states are 27.5 and 22.8 kJ/mol, respectively, those for TS-C and TS-Osp^2, which show a larger asynchronicity in the water-dissociation and OH addition motions, are higher: 44.5 and 74.2 kJ/mol, respectively. The transition state energies for the gas−surface TS-Osp^3 and TS-F pathways compare favorably with the room-temperature activation enthalpy determined experimentally from the solution-phase base hydrolysis of GB (41 kJ/mol).[50] They also compare favorably with the calculated values at various levels of theory for the OH^- + GB reaction including implicit solvation (also ∼40 kJ/mol).[19]

Pentacoordinated Intermediates. Following each of the four minimum energy reaction pathways toward products, we have located four pentacoordinated intermediates with trigonal bipyramidal shape around the central phosphorus atom, shown in Figure 6. All of the intermediates share similarities, but differ in how they are bound to the CsPONb and in the groups that are in axial positions. The pentacoordinated intermediates are bound to the protonated CsPONb through at least two

DOI: 10.1021/acs.jpcc.6b05528
J. Phys. Chem. C 2016, 120, 16822−16830

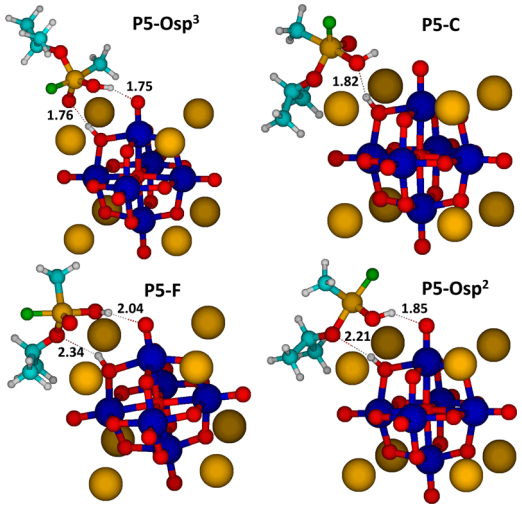

Figure 6. Pentacoordinated intermediates generated in the hydrolysis of GB by $Cs_8Nb_6O_{19}$ along the same four pathways as the minima and transition states of Figures 3 and 4. Numbers correspond to representative hydrogen bond distances in Angstroms. Same color code as in Figure 1.

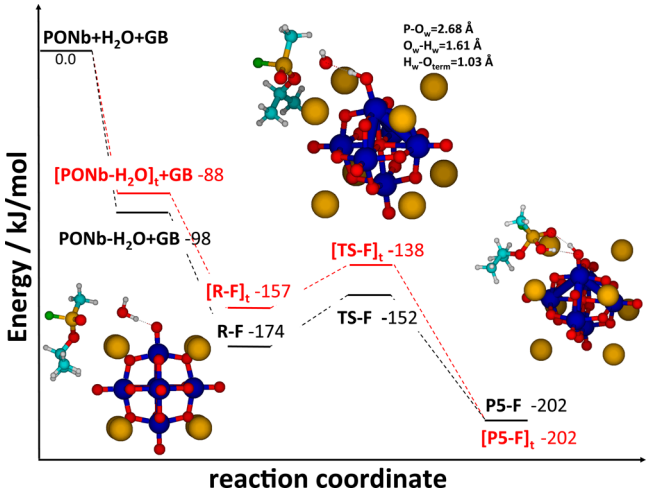

Figure 7. Potential-energy profile for the hydrolysis of GB with $Cs_8Nb_6O_{19}$ along the pathways that place the F group of GB in axial position at the transition state. The red trace is for reaction at the $O_{terminal}$ atom of the CsPONb, and the black trace is for reaction at the $O_{bridging}$ atom. See the text for the nomenclature used to label the various stationary points. The insets are for reaction at the $O_{terminal}$ site and use the same color code as Figure 1.

hydrogen bonds: one between the newly formed phosphonic acid OH group and an $O_{terminal}$ atom in the CsPONb (which is inherited from the transition state), and another one between an electron-rich atom of GB and the H−$O_{bridging}$ group of the CsPONb. In addition to these hydrogen bonds, further interactions contribute to the stability of these P5-CsPONb adducts, including electrostatic contacts between Cs counterions and electron-rich atoms in the intermediate (highlighted in Figure S4), two hydrogen bonds between the $-CH_3$ groups in the isopropoxy of moiety and an $O_{terminal}$ atom (present in all complexes except P5-Osp^3), and a hydrogen bond between the P-CH_3 group and an $O_{terminal}$ atom in P5-Osp^3. The rank in terms of overall stability of these complexes is P5-Osp^2 > P5-F > P5-Osp^3 > P5-C.

In all of the structures except for P5-C, the F atom is in an axial position. However, the former O-sp^2 atom is never axial. These two atoms likely represent the two extrema in the scale of apicophilicity of all the groups bound to the central phosphorus atom examined in this work, which is useful in selecting the lowest-energy path when investigating reaction at the $O_{terminal}$ atom, to which we now turn our attention, and in calculations with explicit crystallization water molecules that we present below.

Reaction at the $O_{terminal}$ Site. The reaction pathways examined until now all involve water dissociation at an $O_{bridging}$ site. This is the most basic site of the CsPONb,[51] and it also participates in the most stable CsPONb−H_2O complex. However, reaction at the $O_{terminal}$ site can also occur. To examine this possibility, we have mapped the likely lowest-energy reaction path departing from the CsPONb−H_2O complex that has a water molecule hydrogen bonding to only the terminal O atom (Figure S1). Using the apicophilicity scale derived from reaction at the bridging site in the prior section, we have assumed that reaction in which the P−F bond of the nerve agent is collinear to the P−OH bond that is forming in the transition state of the rate-determining step is the likely lowest-energy reaction path.

Figure 7 presents the potential energy profile of the rate-determining step for reaction at the $O_{terminal}$ site in comparison with the same path at the $O_{bridging}$ site reported above. The energies of the stationary points for reaction at the $O_{terminal}$ site tend to be higher in energy than at the $O_{bridging}$ site. This seems to be a consequence of the more peripheral nature of the $O_{terminal}$ site, which does not allow for as strong interactions between the GB atoms and the CsPONb as the more internal $O_{bridging}$ site. Notwithstanding, the barrier for reaction from the R-F complex is comparable for reaction at both the bridging and terminal sites. The Lindqvist ion has twice as many $O_{bridging}$ sites as $O_{terminal}$ sites, but the similarity of the barriers obtained in this work suggest that hydrolysis of GB with CsPONb might take place at both sites. While we have not studied the energy paths for reactions at the terminal O atom along the other three approaches of GB to the PONb, we expect that the trends for reaction at the $O_{terminal}$ site seen here will likely extend to those other paths.

Pentacoordinated Intermediate Dissociation. Once the pentacoordinated species is formed, reaction will progress along three reaction paths. First, Berry pseudorotation of the trigonal bipyramidal intermediate might occur, as has been reported in bulk hydrolysis calculations of OP compounds using implicit solvent models.[52] In this pseudorotation, groups with the largest apicophilicity are directed to the axial positions. Second, the intermediate might dissociate unimolecularly, without the involvement of the catalyst. Support for this mechanism is also provided by earlier computational studies of the OH^- + GB reaction with implicit solvation, which reported that dissociation of the pentacoordinated intermediate to generate F atoms occurs over very low barriers and is not rate-limiting.[18,19] This unimolecular dissociation can be competitive with the pseudorotation pathway. While those rapid pseudorotation and autodissociation pathways will likely be present in the pentacoordinated intermediates bound to the CsPONb located in this work, we have examined a third set of pathways that involve the catalyst in order to evaluate the prospect of a fully catalytic process.

There are two major dissociation pathways for the pentacoordinated intermediate: F elimination and isopropoxy

DOI: 10.1021/acs.jpcc.6b05528
J. Phys. Chem. C 2016, 120, 16822−16830

elimination. The accompanying products are isopropyl methyl phosphonic acid (IMPA) and methyl phosphonofluoridic acid (MPFA), respectively. In order to obtain full regeneration of the catalyst, the nascent F or isopropoxy groups need to abstract the proton that remains bound to the $O_{bridging}$ site as a consequence of the hydrolysis reaction (see Figure 6). We have therefore attempted to locate transition states that lead either to HF and IMPA or isopropanol (iPOH) and MPFA from the most stable pentacoordinated intermediates.

Transition states have been obtained for the reaction that decomposes P5-F and P5-Osp^2 to iPOH and MPFA. The structures are shown in Figure 8, and the energies of these

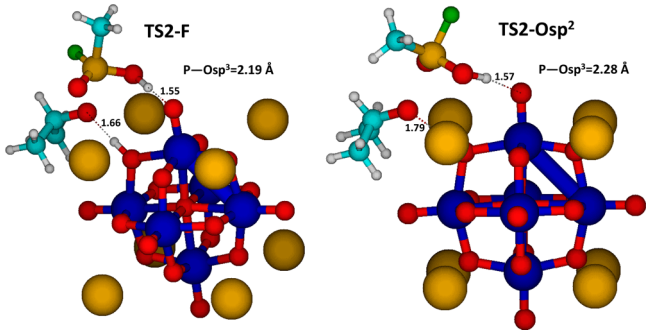

Figure 8. Transition states for the decomposition of the P5-F and P5-Osp^2 intermediates generated in the hydrolysis reaction of GB by $Cs_8Nb_6O_{19}$. Values correspond to representative hydrogen-bond distances in Angstroms. Additional distances are available in Figure S5. Same color code as in Figure 1.

transition states referred to their corresponding pentacoordinated intermediates are 24.9 kJ/mol for TS2-F and 3.1 kJ/mol for TS2-Osp^2. The difference in the barrier seems associated with the fact that the isopropoxy leaving group in TS2-F is initially in an equatorial position in P5-F, and a pseudorotation that places the group in an axial position needs to occur,[52] which carries an energetic penalty.

All attempts to locate a pentacoordinated intermediate in which the F atom is in an axial position and hydrogen bonded to the H−$O_{bridging}$ group directly led to HF + IMPA products adsorbed on the PONb. The potential energy during these failed geometry optimization attempts was steeply downhill, suggesting that P−F dissociation likely occurs through a small barrier or is entirely barrierless. This is consistent with the very small barrier for this dissociation channel found in prior implicit solvation calculations (1.3 kJ/mol).[19]

The main conclusion of the results presented in this section is that the pentacoordinated species generated in the rate-limiting step of the hydrolysis reaction of GB by CsPONb undergo fast dissociation to HF + IMPA and iPOH + MPFA. This process can take place without the involvement of the catalyst, as shown in prior work, or it can involve the proton transferred from water to an $O_{bridging}$ site of the PONb in the rate-determining step, as revealed in this work. These processes might occur concurrently with the interconversion between pentacoordinated isomers through Berry pseudorotation.

Products. The facile dissociation of the P5 species involving the catalyst yields HF and IMPA or iPOH and MPFA products. All these species are initially bound to the CsPONb, as shown in Figure 9. The CsPONb−IMPA−HF complex exhibits an HF molecule forming a hydrogen bond with the $O_{bridging}$ atom that has played a central role in the hydrolysis reaction, and an

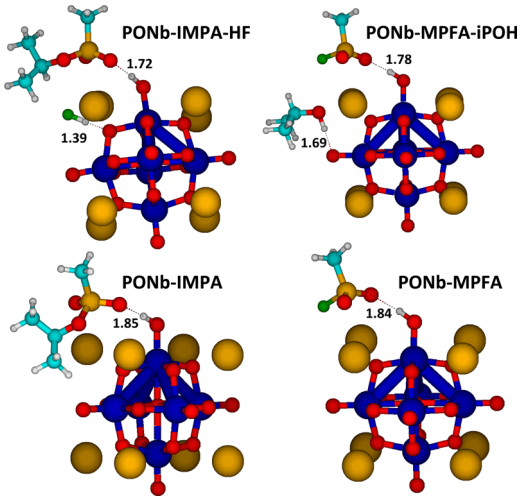

Figure 9. Bound products in the hydrolysis reaction of GB with $Cs_8Nb_6O_{19}$. Numbers correspond to representative hydrogen-bond distances in Angstroms. Same color code as in Figure 1.

IMPA molecule hydrogen bonded to an $O_{terminal}$ atom. Additional interactions exist, including close contacts between the Cs ions of the PONb and the electronegative atoms of IMPA (Figure S6), and a hydrogen bond between C−H bonds in the isopropoxy group of IMPA and the F atom of the adsorbed HF. The bound products that stem from the P−O dissociation of P5 complexes (CsPONb−MPFA−iPOH) consist of an isopropanol molecule hydrogen bonded to an $O_{terminal}$ atom, and MPFA bound to a neighboring $O_{terminal}$ atom. Following the minimum energy reaction path of the dissociation through TS2-Osp^2 initially leads to isopropanol forming a hydrogen bond with the $O_{bridging}$ atom, much as shown for HF in the CsPONb−IMPA−HF complex. However, repulsion between the adsorbed MPFA and iPOH causes the migration of isopropanol from the $O_{bridging}$ atom to a vicinal $O_{terminal}$ atom, as shown in Figure 9. A similar migration was seen in reactions with organosilyl reagents and the Lindqvist complex, $Nb_2W_4O_{19}H^{3-}$.[53]

CsPONb−MPFA−iPOH is the overall lowest-energy structure of all 22 stationary points of the reaction mechanism in Figure 2. The high stability of this complex is due in part to the strong hydrogen bonds between the adsorbates and the CsPONb, but also to the additional stabilizing interactions between the Cs counterions and electronegative atoms of the nerve-agent fragments (Figure S6). These interactions are also present in CsPONb−IMPA−HF.

Desorption of HF (66.3 kJ/mol binding energy) and isopropanol (75.5 kJ/mol) generates CsPONb−IMPA and CsPONb−MPFA adducts, respectively. The phosphonic acids are extraordinarily strongly bound to the PONb, by 251.3 kJ/mol in the case of IMPA and 262.9 kJ/mol for MPFA. The structure of these tightly bound complexes is also shown in Figure 9. Noticeably, even though the protonated phosphonic acids and deprotonated CsPONb separated products are more stable than the corresponding phosphonate + protonated CsPONb products, Figure 9 shows that there is a proton transfer from the phosphonic acids to an $O_{terminal}$ atom of the CsPONb while they are interacting. This proton transfer is already present when HF and isopropanol are still bound to the CsPONb. The reason for the proton transfer seems to be rooted in the ability of the phosphonates to establish stronger

DOI: 10.1021/acs.jpcc.6b05528
J. Phys. Chem. C 2016, 120, 16822−16830

interactions with neighboring Cs counterions than if the IMPA and MPFA species are protonated. For deprotonated MPFA bound to the protonated CsPONb, aside from the hydrogen bond between the $O_{terminal}$−H group of the CsPONb and one of the oxygen atoms of MPFA, we see various electrostatic contacts between the two oxygen atoms and the fluorine atom in MPFA and neighboring Cs ions (Figure S6). In the case of deprotonated IMPA bound to the protonated CsPONb, the hydrogen bond is also assisted by contacts between the three oxygen atoms and Cs ions and by a hydrogen bond between a $-CH_3$ group in the isopropoxy moiety and an $O_{terminal}$ atom. The large binding energies between the phosphonate products obtained in this work and the catalyst imply that full regeneration of the catalyst as modeled in this work will likely require the supply of thermal energy.

Effect of Explicit Solvation. All calculations presented so far consider that the catalyst is a dry hexaniobate. However, even in solid form, CsPONb contains crystallization water molecules.[42] To investigate the effect of hydration on the mechanism of nerve-agent hydrolysis, we have conducted calculations for the minimum-energy reaction path with a CsPONb hydrated with 14 water molecules, which are treated explicitly at the same level of theory as the calculations reported above.

The starting catalyst structure in the calculations was taken from the X-ray diffraction data of the $Cs_8Nb_6O_{19}\cdot 14H_2O$ salt described in the experiment.[42] After full geometry optimization, we note that all 14 water molecules are forming hydrogen bonds with O atoms in the niobate and also solvating the Cs ions. Hydration has a slight effect on the structure of the hexaniobate core, which no longer possesses octahedral point-group symmetry. The average Nb−$O_{central}$ and Nb−$O_{bridging}$ atoms are 0.015 and 0.020 Å shorter than in the dry CsPONb, and the average Nb−$O_{terminal}$ distance is 0.026 Å longer. The most notable difference between the hydrated and dry CsPONb structure is in the average Cs−$O_{bridging}$ nearest-neighbor distance, which increases by 0.232 Å in the hydrated catalyst. It therefore seems that the main effect of crystallization water in the catalyst is to screen the interactions between the Cs counterions and the hexaniobate core.

Figure 10 shows the potential energy surface for the "F" pathway with the hydrated CsPONb in comparison with the results for the same pathway presented in Figure 2 for the dry catalyst. The potential profile in Figure 10 shows that explicit inclusion of crystallization waters does not affect the reaction mechanism of nerve agent hydrolysis and suggests that the water molecules that are not undergoing dissociation seem to have an attending or spectator role in the mechanism. The attending water molecules do, however, noticeably affect the energetics of the reaction, and intermediates and transition states are all shifted up in energy compared to those in the dry catalyst. This energy offset appears to be a consequence of the screening effect of the interactions between the CsPONb and the H_2O and GB reagents by the nonreactive water molecules. For instance, the binding of the H_2O molecule that dissociates during reaction is 20 kJ/mol less exothermic in the hydrated CsPONb than in the dry one. Likewise, GB binds 21 kJ/mol less tightly on the hydrated CsPONb than to the dry one. After both H_2O and GB are bound, the rate-limiting step has a barrier of 31 kJ/mol, which is slightly higher than with the dry CsPONb (23 kJ/mol), but still lower than the activation energy measured experimentally for bulk hydrolysis with hydroxide ions (41 kJ/mol).

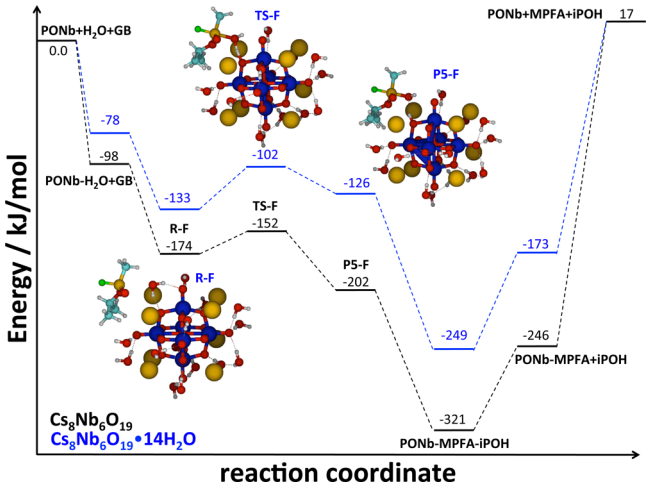

Figure 10. Potential energy profile for the hydrolysis of GB with $Cs_8Nb_6O_{19}$ (black trace) and $Cs_8Nb_6O_{19}\cdot 14H_2O$ (blue trace) along the minimum-energy reaction path. See the text for the nomenclature used to label the various stationary points. The insets are for reaction $Cs_8Nb_6O_{19}\cdot 14H_2O$ and use the same color code as Figure 1.

Beyond the transition state, we note that the rest of stationary points in the hydrated system are about 75 kJ/mol less stable than in the dry catalyst. Notwithstanding, the desorption of the phosphonic acid generated during reaction (MPFA in Figure 10) from the catalyst still requires a significant amount of energy (190 kJ/mol), suggesting the likely need for thermal treatment to regenerate the catalyst.

CONCLUDING REMARKS

This work presents the potential energy profile for the decomposition of GB by a hexaniobate catalyst whose reactivity has been recently proven experimentally. The early steps of the reaction mechanism involve the adsorption of water and the nerve agent on the $Cs_8Nb_6O_{19}$ catalyst. Both molecules bind to the catalyst through a variety of intermolecular interactions that include hydrogen bonds and electrostatic interactions involving the Cs counterions. Once the reagents are bound, the ensuing rate-determining step is a concerted dissociation of the adsorbed water molecule on a basic oxygen atom of the catalyst and nucleophilic addition of the nascent OH group to the nerve agent. The location of transition states for this concerted process in this work confirms a recent proposal from SAXS measurements and provides fundamental insight into the general base hydrolysis mechanism of nerve agents on solid-state catalysts. The calculated transition-state energies for reaction with the $Cs_8Nb_6O_{19}$ catalyst are well below the fully separated reagents' asymptote. Even if none of the energy released in the formation of the CsPONb−H_2O−GB complexes can be utilized to surmount the barrier, some of the barriers for reaction from these complexes are sufficiently small that thermal reaction can occur rapidly at room temperature. Remarkably, some of the calculated reaction barriers are notably smaller than the activation energy determined experimentally in bulk hydrolysis of GB, which encourages further study of hexaniobate catalysts for base hydrolysis of nerve agents.

The rate-determining step results in pentacoordinated intermediates that undergo rapid subsequent dissociation. This dissociation might occur without participation of the catalyst, as has been reported in earlier studies, or with

DOI: 10.1021/acs.jpcc.6b05528
J. Phys. Chem. C 2016, 120, 16822−16830

involvement of the catalyst as calculated here; both processes possess very low barriers. The products of the pentacoordinated intermediate decomposition assisted by the catalyst are either HF + IMPA or iPOH + MPFA. These products are strongly bound to the catalyst through hydrogen bonds and electrostatic interactions with the Cs counterions, suggesting that full catalyst regeneration might entail thermal treatment.

Inclusion of crystallization water molecules in the calculations does not alter the steps of the reaction mechanism, but does influence the energy of the stationary points. The attending water molecules act to screen the interactions between the Cs counterions, the hexaniobate core, and all species bound to the catalyst, which results in an upward shift of the stationary point energies with respect to the dry catalyst.

While the results presented in this article support recent experimental findings, a more quantitative connection between the calculations and the experiment is not possible at this time. From the experimental perspective, neither the activation energy nor the characterization of intermediates is available. From the calculations point of view, the energies have been obtained with a moderate basis set due to the system size and will necessarily show some deviation from experiment. In addition, the energies seem highly dependent on the level of hydration of the catalyst, which might challenge a quantitative comparison between theory and experiment.

Finally, the discovery in this work of the prominent role played by the Cs ions in stabilizing many of the adsorbed species on the catalyst will warrant additional studies that target the effect of other monovalent counterions of the PONb on the potential energy surface. In conjunction to the seminal mechanistic work presented here, that work will aim to design optimum solid-state catalysts for decontamination of nerve agents.

■ ASSOCIATED CONTENT

Supporting Information

The Supporting Information is available free of charge on the ACS Publications website at DOI: 10.1021/acs.jpcc.6b05528.

Structures of minima and transition states; Gibbs energies of stationary points; atomic Cartesian coordinates of stationary points (PDF)

Animations of atomic motions along minimum energy reaction path merp-F (MPG)

Animations of atomic motions along minimum energy reaction path merp-Osp^3 (MPG)

Animations of atomic motions along minimum energy reaction path merp-CH_3 (MPG)

Animations of atomic motions along minimum energy reaction path merp-Osp^2 (MPG)

■ AUTHOR INFORMATION

Corresponding Author

*E-mail: troya@vt.edu. Phone: +1 540 231 1381.

Notes

The authors declare no competing financial interest.

■ ACKNOWLEDGMENTS

This material is based upon work supported by the U.S. Army Research Laboratory and the U.S. Army Research Office under grant number W911NF-15-2-0107. The authors are grateful for support of the Defense Threat Reduction Agency. The authors wish to thank May Nyman for providing cif files with the crystal structure of the CsPONb used in this work. The authors acknowledge Advanced Research Computing at Virginia Tech for providing computational resources and technical support that have contributed to the results reported within this paper.

■ REFERENCES

(1) Kim, K.; Tsay, O. G.; Atwood, D. A.; Churchill, D. G. Destruction and Detection of Chemical Warfare Agents. *Chem. Rev.* **2011**, *111*, 5345−5403.

(2) Jang, Y. J.; Kim, K.; Tsay, O. G.; Atwood, D. A.; Churchill, D. G. Update 1 Of: Destruction and Detection of Chemical Warfare Agents. *Chem. Rev.* **2015**, *115*, PR1−PR76.

(3) Yang, Y. C.; Baker, J. A.; Ward, J. R. Decontamination of Chemical Warfare Agents. *Chem. Rev.* **1992**, *92*, 1729−1743.

(4) Bandosz, T. J.; Laskoski, M.; Mahle, J.; Mogilevsky, G.; Peterson, G. W.; Rossin, J. A.; Wagner, G. W. Reactions of VX, GD, and HD with $Zr(OH)_4$: Near Instantaneous Decontamination of VX. *J. Phys. Chem. C* **2012**, *116*, 11606−11614.

(5) Yang, S. W.; Doetschman, D. C.; Schulte, J. T.; Sarnbur, J. B.; Kanyi, C. W.; Fox, J. D. Sodium X-Type Faujasite Zeolite Decomposition of Dimethyl Methylphosphonate (DMMP) to Methylphosphonate: Nucleophilic Zeolite Reactions I. *Microporous Mesoporous Mater.* **2006**, *92*, 56−60.

(6) Bromberg, L.; Schreuder-Gibson, H.; Creasy, W. R.; McGarvey, D. J.; Fry, R. A.; Hatton, T. A. Degradation of Chemical Warfare Agents by Reactive Polymers. *Ind. Eng. Chem. Res.* **2009**, *48*, 1650−1659.

(7) Kinnan, M. K.; Creasy, W. R.; Fullmer, L. B.; Schreuder-Gibson, H. L.; Nyman, M. Nerve Agent Degradation with Polyoxoniobates. *Eur. J. Inorg. Chem.* **2014**, *2014*, 2361−2367.

(8) Guo, W.; Lv, H.; Sullivan, K. P.; Gordon, W. O.; Balboa, A.; Wagner, G. W.; Musaev, D. G.; Bacsa, J.; Hill, C. L. Broad-Spectrum Liquid- and Gas-Phase Decontamination of Chemical Warfare Agents by One-Dimensional Heteropolyniobates. *Angew. Chem., Int. Ed.* **2016**, *55*, 7403−7407.

(9) DeCoste, J. B.; Peterson, G. W. Metal−Organic Frameworks for Air Purification of Toxic Chemicals. *Chem. Rev.* **2014**, *114*, 5695−5727.

(10) Moon, S. Y.; Wagner, G. W.; Mondloch, J. E.; Peterson, G. W.; DeCoste, J. B.; Hupp, J. T.; Farha, O. K. Effective, Facile, and Selective Hydrolysis of the Chemical Warfare Agent VX Using Zr_6-Based Metal-Organic Frameworks. *Inorg. Chem.* **2015**, *54*, 10829−10833.

(11) Liu, Y.; Moon, S. Y.; Hupp, J. T.; Farha, O. K. Dual-Function Metal-Organic Framework as a Versatile Catalyst for Detoxifying Chemical Warfare Agent Simulants. *ACS Nano* **2015**, *9*, 12358−12364.

(12) Mondloch, J. E.; Katz, M. J.; Isley, W. C.; Ghosh, P.; Liao, P. L.; Bury, W.; Wagner, G.; Hall, M. G.; DeCoste, J. B.; Peterson, G. W.; et al. Destruction of Chemical Warfare Agents Using Metal-Organic Frameworks. *Nat. Mater.* **2015**, *14*, 512−516.

(13) Katz, M. J.; Mondloch, J. E.; Totten, R. K.; Park, J. K.; Nguyen, S. T.; Farha, O. K.; Hupp, J. T. Simple and Compelling Biomimetic Metal-Organic Framework Catalyst for the Degradation of Nerve Agent Simulants. *Angew. Chem., Int. Ed.* **2014**, *53*, 497−501.

(14) Song, J.; Luo, Z.; Britt, D. K.; Furukawa, H.; Yaghi, O. M.; Hardcastle, K. I.; Hill, C. L. A Multiunit Catalyst with Synergistic Stability and Reactivity: A Polyoxometalate−Metal Organic Framework for Aerobic Decontamination. *J. Am. Chem. Soc.* **2011**, *133*, 16839−16846.

(15) Ma, F. J.; Liu, S. X.; Sun, C. Y.; Liang, D. D.; Ren, G. J.; Wei, F.; Chen, Y. G.; Su, Z. M. A Sodalite-Type Porous Metal-Organic Framework with Polyoxometalate Templates: Adsorption and Decomposition of Dimethyl Methylphosphonate. *J. Am. Chem. Soc.* **2011**, *133*, 4178−4181.

(16) Rando, R. R. Mechanisms of Action of Naturally Occurring Irreversible Enzyme Inhibitors. *Acc. Chem. Res.* **1975**, *8*, 281−288.

(17) Zheng, F.; Zhan, C.-G.; Ornstein, R. L. Theoretical Studies of Reaction Pathways and Energy Barriers for Alkaline Hydrolysis of Phosphotriesterase Substrates Paraoxon and Related Toxic Phospho-

DOI: 10.1021/acs.jpcc.6b05528
J. Phys. Chem. C 2016, 120, 16822−16830

fluoridate Nerve Agents. *J. Chem. Soc., Perkin Trans. 2* **2001**, 2355−2363.
(18) Dyguda-Kazimierowicz, E.; Sokalski, W. A.; Leszczynski, J. Gas-Phase Mechanisms of Degradation of Hazardous Organophosphorus Compounds: Do They Follow a Common Pattern of Alkaline Hydrolysis Reaction as in Phosphotriesterase? *J. Phys. Chem. B* **2008**, *112*, 9982−9991.
(19) Šečkutė, J.; Menke, J. L.; Emnett, R. J.; Patterson, E. V.; Cramer, C. J. Ab Initio Molecular Orbital and Density Functional Studies on the Solvolysis of Sarin and O,S-Dimethyl Methylphosphonothiolate, a VX-Like Compound. *J. Org. Chem.* **2005**, *70*, 8649−8660.
(20) Poblet, J. M.; Lopez, X.; Bo, C. Ab Initio and DFT Modelling of Complex Materials: Towards the Understanding of Electronic and Magnetic Properties of Polyoxometalates. *Chem. Soc. Rev.* **2003**, *32*, 297−308.
(21) Miro, P.; Poblet, J. M.; Avalos, J. B.; Bo, C. Towards a Computational Treatment of Polyoxometalates in Solution Using QM Methods and Explicit Solvent Molecules. *Can. J. Chem.* **2009**, *87*, 1296−1301.
(22) Bo, C.; Poblet, J. M. Electronic Properties and Molecular Simulations of Polyoxometalates. *Isr. J. Chem.* **2011**, *51*, 228−237.
(23) Lopez, X.; Miro, P.; Carbo, J. J.; Rodriguez-Fortea, A.; Bo, C.; Poblet, J. M. Current Trends in the Computational Modelling of Polyoxometalates. *Theor. Chem. Acc.* **2011**, *128*, 393−404.
(24) Lopez, X.; Carbo, J. J.; Bo, C.; Poblet, J. M. Structure, Properties and Reactivity of Polyoxometalates: A Theoretical Perspective. *Chem. Soc. Rev.* **2012**, *41*, 7537−7571.
(25) Matt, B.; Xiang, X.; Kaledin, A. L.; Han, N. N.; Moussa, J.; Amouri, H.; Alves, S.; Hill, C. L.; Lian, T. Q.; Musaev, D. G.; et al. Long Lived Charge Separation in Iridium(III)-Photosensitized Polyoxometalates: Synthesis, Photophysical and Computational Studies of Organometallic-Redox Tunable Oxide Assemblies. *Chem. Sci.* **2013**, *4*, 1737−1745.
(26) Kuznetsov, A. E.; Geletii, Y. V.; Hill, C. L.; Morokuma, K.; Musaev, D. G. Dioxygen and Water Activation Processes on Multi-Ru-Substituted Polyoxometalates: Comparison with the "Blue-Dimer" Water Oxidation Catalyst. *J. Am. Chem. Soc.* **2009**, *131*, 6844−6854.
(27) Hill, C. L.; Prosser-McCartha, C. M. Homogeneous Catalysis by Transition Metal Oxygen Anion Clusters. *Coord. Chem. Rev.* **1995**, *143*, 407−455.
(28) Cronin, L.; Muller, A. From Serendipity to Design of Polyoxometalates at the Nanoscale, Aesthetic Beauty and Applications. *Chem. Soc. Rev.* **2012**, *41*, 7333−7334.
(29) Long, D.-L.; Tsunashima, R.; Cronin, L. Polyoxometalates: Building Blocks for Functional Nanoscale Systems. *Angew. Chem., Int. Ed.* **2010**, *49*, 1736−1758.
(30) Long, D.-L.; Tsunashima, R.; Cronin, L. Polyoxometallate Als Bausteine Für Funktionelle Nanosysteme. *Angew. Chem.* **2010**, *122*, 1780−1803.
(31) Borrás-Almenar, J. J.; Coronado, E.; Müller, A.; Pope, M. *Polyoxometalate Molecular Science. Proceedings of the Nato Advanced Study Institute*, Tenerife, Spain from 25 August to 4 September 2001; Kluwer Academic Publishers: Dordrecht, 2003; Vol. *98*.
(32) Hill, C. L. Introduction: Polyoxometalates–Multicomponent Molecular Vehicles to Probe Fundamental Issues and Practical Problems. *Chem. Rev.* **1998**, *98*, 1−2.
(33) Pope, M. T.; Müller, A. Chemie Der Polyoxometallate: Aktuelle Variationen Über Ein Altes Thema Mit Interdisziplinären Bezügen. *Angew. Chem.* **1991**, *103*, 56−70.
(34) Pope, M. T.; Müller, A. Polyoxometalate Chemistry: An Old Field with New Dimensions in Several Disciplines. *Angew. Chem., Int. Ed. Engl.* **1991**, *30*, 34−48.
(35) Hill, C. L. Progress and Challenges in Polyoxometalate-Based Catalysis and Catalytic Materials Chemistry. *J. Mol. Catal. A: Chem.* **2007**, *262*, 2−6.
(36) Neumann, R. In *Prog. Inorg. Chem.*; John Wiley & Sons, Inc., 2007; pp 317−370.
(37) Nyman, M. Polyoxoniobate Chemistry in the 21st Century. *Dalton Trans.* **2011**, *40*, 8049−8058.
(38) Bridgeman, A. J.; Cavigliasso, G. Structure and Bonding in $[M_6O_{19}]^{n-}$ Isopolyanions. *Inorg. Chem.* **2002**, *41*, 1761−1770.
(39) Black, J. R.; Nyman, M.; Casey, W. H. Rates of Oxygen Exchange between the $[H_xNb_6O_{19}]^{(8-x)}{}_{(aq)}$ Lindqvist Ion and Aqueous Solutions. *J. Am. Chem. Soc.* **2006**, *128*, 14712−14720.
(40) Kaledin, A. L.; van Duin, A. C. T.; Hill, C. L.; Musaev, D. G. Parameterization of Reactive Force Field: Dynamics of the $[Nb_6O_{19}H_x]^{(8-x)-}$ Lindqvist Polyoxoanion in Bulk Water. *J. Phys. Chem. A* **2013**, *117*, 6967−6974.
(41) Anderson, T. M.; Rodriguez, M. A.; Bonhomme, F.; Bixler, J. N.; Alama, T. M.; Nyman, M. An Aqueous Route to $[Ta_6O_{19}]^{8-}$ and Solid-State Studies of Isostructural Niobium and Tantalum Oxide Complexes. *Dalton Trans.* **2007**, 4517−4522.
(42) Nyman, M.; Alam, T. M.; Bonhomme, F.; Rodriguez, M. A.; Frazer, C. S.; Welk, M. E. Solid-State Structures and Solution Behavior of Alkali Salts of the $[Nb_6O_{19}]^{8-}$ Lindqvist Ion. *J. Cluster Sci.* **2006**, *17*, 197−219.
(43) Antonio, M. R.; Nyman, M.; Anderson, T. M. Direct Observation of Contact Ion-Pair Formation in Aqueous Solution. *Angew. Chem., Int. Ed.* **2009**, *48*, 6136−6140.
(44) Fullmer, L. B.; Molina, P. I.; Antonio, M. R.; Nyman, M. Contrasting Ion-Association Behaviour of Ta and Nb Polyoxometalates. *Dalton Trans.* **2014**, *43*, 15295−15299.
(45) Frisch, M. J.; Trucks, G. W.; Schlegel, H. B.; Scuseria, G. E.; Robb, M. A.; Cheeseman, J. R.; Scalmani, G.; Barone, V.; Mennucci, B.; Petersson, G. A.; et al. *Gaussian 09*, revision E.01; Gaussian, Inc.: Wallingford, CT, 2009.
(46) Zhao, Y.; Truhlar, D. G. A New Local Density Functional for Main-Group Thermochemistry, Transition Metal Bonding, Thermochemical Kinetics, and Noncovalent Interactions. *J. Chem. Phys.* **2006**, *125*, 194101.
(47) Alam, T. M.; Nyman, M.; Cherry, B. R.; Segall, J. M.; Lybarger, L. E. Multinuclear Nmr Investigations of the Oxygen, Water, and Hydroxyl Environments in Sodium Hexaniobate. *J. Am. Chem. Soc.* **2004**, *126*, 5610−5620.
(48) Benschop, H. P.; De Jong, L. P. A. Nerve Agent Stereoisomers: Analysis, Isolation and Toxicology. *Acc. Chem. Res.* **1988**, *21*, 368−374.
(49) Buono, G.; Llinas, J. R. Oxyphosphoranes with an Oxaphospholene Ring: Analysis of the Activation Barriers of the Isomerization Process. *J. Am. Chem. Soc.* **1981**, *103*, 4532−4540.
(50) Gustafson, R. L.; Martell, A. E. A Kinetic Study of the Copper(II) Chelate-Catalyzed Hydrolysis of Isopropyl Methylphosphonofluoridate (Sarin). *J. Am. Chem. Soc.* **1962**, *84*, 2309−2316.
(51) Balogh, E.; Anderson, T. M.; Rustad, J. R.; Nyman, M.; Casey, W. H. Rates of Oxygen-Isotope Exchange between Sites in the $[H_xTa_6O_{19}]^{(8-x)-}{}_{(aq)}$ Lindqvist Ion and Aqueous Solutions: Comparisons to $[H_xNb_6O_{19}]^{(8-x)-}{}_{(aq)}$. *Inorg. Chem.* **2007**, *46*, 7032−7039.
(52) Daniel, K. A.; Kopff, L. A.; Patterson, E. V. Computational Studies on the Solvolysis of the Chemical Warfare Agent VX. *J. Phys. Org. Chem.* **2008**, *21*, 321−328.
(53) Day, V. W.; Klemperer, W. G.; Schwartz, C. Synthesis, Characterization, and Interconversion of the Niobotungstic Acid $Nb_2W_4O_{19}H^{3-}$ and Its Anhydride and Alkyl/Silyl Esters. *J. Am. Chem. Soc.* **1987**, *109*, 6030−6044.

DOI: 10.1021/acs.jpcc.6b05528
J. Phys. Chem. C 2016, 120, 16822−16830